Hindawi
Advances in Civil Engineering
Volume 2021, Article ID 8874655, 15 pages
https://doi.org/10.1155/2021/8874655

Research Article

Experimental Study on Mechanical Properties of Reinforced Soil Interface under Dry-Wet Cycle

Liang Huang,[1] Wenbo Ma,[1] Yujie Hou,[2] Bo Wang,[2] and Jiahua Zhu[2]

[1]*School of Civil Engineering, Zhengzhou University, Zhengzhou 450000, China*
[2]*School of Water Conservancy Engineering, Zhengzhou University, Zhengzhou 450000, China*

Correspondence should be addressed to Yujie Hou; houyujie@yeah.net

Received 30 June 2020; Revised 31 December 2020; Accepted 7 January 2021; Published 20 January 2021

Academic Editor: Castorina S. Vieira

The reinforced soil-retaining wall has been widely used in coastal projects, and the dry-wet cycles influence the mechanical properties of the reinforced soil interface. This study conducts macro-micro tests and selects four different water content samples of reinforced soil with five types of overburden pressure conditions and three sets of dry-wet cycles, with a total of 60 working conditions. The pull-out test was used to study the mechanical properties of the reinforced soil interface. The scanning electron microscope was used to observe the microscopic characterization of the particles under different working conditions. Through the analysis of the experimental results, we can draw the conclusion as follows. (1) The friction coefficient of the reinforced soil interface decreases with the increase of the number of dry and wet cycles. (2) The apparent cohesion of soil-reinforcement interface decreases with the increase of the number of dry-wet cycles. After 30 dry-wet cycles, the apparent cohesion of the soil-reinforcement interface with water content of 14% is the maximum 5.91 kPa. The variation law of cohesion derived from microstructure analysis conforms to the laws and conclusions obtained by the experiment. (3) The shear stress of the reinforced soil is linearly related to the normal stress, which is in accordance with Coulomb's law.

1. Introduction

The reinforced soil-retaining wall has been widely used in coastal projects because of its small area, lower cost, and simple construction. However, the wet-dry cycles have a great impact on the mechanical properties of the reinforced soil, which can cause damage to the structure and reduce the dynamic strength. Many scholars [1–7] have conducted research studies on the changes of mechanical properties of different soils after dry-wet cycles. Under the action of the dry-wet cycle, the shear strength of the solidified light-weight soil decreases significantly at the beginning of shearing and then stabilizes. As the number of undisturbed loess dry-wet cycles increases, the porosity of soil gradually increases, and the liquid limit and plasticity index decrease successively, while the plastic limit remains basically unchanged. The shear strength of red clay will decrease under the action of dry-wet cycles. With the increase of the number of dry-wet cycles, the attenuation rate of shear strength first decreases and then stabilizes finally. The dynamic strength and dynamic strength indexes of compacted loess first decrease and then increase gradually with the increase of the number of dry-wet cycles. Affected by the amplitude of the dry-wet cycles, the turning point of the curve is obviously different. The curves of shear stress, normal stress, and shear displacement at the reinforced soil interface develop in the form of "hysteresis loop" and "dish," respectively. As the number of dry-wet cycles increases, the attenuation rate decreases gradually, and the peak values appear at the maximum displacement. With the increase of the dry-wet cycle number, the shear strength and cohesive force of the modified soil gradually decrease, and the no-load expansion rate becomes stable after increasing. The changes in mechanical properties of silty clay under saturated conditions are related to the historical drying stress. The greater the historical drying stress, the more obvious the mechanical properties of the soil under saturation changes.

Some scholars have explored the interaction between geogrid and soil. Shao [8] simulated the mechanical properties of the reinforcement-soil interface with the particle flow method and obtained the effect of the geotextile and geogrid under different normal stresses. Pant et al. [9] explored the mechanical properties of coal combustion residues as structural filling materials for reinforced soil structures. Cardile et al. [10] studied the influence of cyclic load history on the interaction of reinforcement and soil. Morsy et al. [11] developed a new device that can comprehensively evaluate the interaction between soil and reinforcement and the relationship between adjacent reinforcement layers in the reinforced soil under working and final interface shear stress conditions. Pinho-Lopes and de Lurdes Lopes [12] studied the impact of laboratory-induced mechanical damage on soil-soil interaction under inclined plane shear. Liu et al. [13] pointed out the limitations of the current domestic standards and believed that the size of the model box in the domestic standards was too small, the test boundary conditions did not meet the actual engineering conditions, and the test pull rates were different, which seriously affected the strength parameters of the reinforcement-soil interface. Then, it summarizes the composition of the drawing resistance of the geogrid, contribution rate of each part, end bearing resistance of the transverse rib, and calculation method of the drawing resistance in detail. Xiao et al. [14] found that the force of the grid during the drawing process is transmissive and uneven. Zhang [15] found that the size of the equipment significantly changes the shear strength of the interface between the reinforcement and soil. Zhang and Lin [16] used the particle flow to study the meso-mechanism of the reinforcement-soil interface of the grid-like toothed reinforced sand cushion structure and analyzed the evolution and load transfer mechanism of the shear band at the drawing interface. Punetha et al. [17] studied the microstructure of the interface mechanical behavior of geosynthetics in direct shear tests. Mousavi et al. [18] studied the shear strength behavior of the interface between contaminated soil and biodiesel and geosynthetics. Tang et al. [19] established a three-dimensional numerical model of the direct shear friction characteristics of the reinforced material (geogrid) interface to study the reduction law of soil strength and the strength of the geogrid interface. Ferreira et al. [20] studied the postcyclic shear behavior of the granite residual soil-geogrid interface. Wan et al. [21] investigated the role of vegetation roots in the stability of landfill clay covers subject to dry-wet cycles. Soil shear strength is tested at different depths of bare and vegetation covers before and after 1 year of seasonal dry-wet cycles. Ferreira et al. [22] conducted a series of large-scale pull-out tests involving different soil moisture and density conditions, evaluating the pull test of three different geosynthetics (geogrids, geocomposite reinforcements, and geotextiles). In order to explore the reinforcement mechanism of glass fiber on red clay, Jiang et al. [23] conducted an indoor unconfined compressive strength test, combined with discrete element technology for numerical analysis, and studied the mechanical properties of the reinforced soil with different fiber content. Through theoretical analysis, indoor and outdoor experimental research, and numerical simulation, Liu [24] systematically studied the interaction mechanism of the reinforcement and soil, the mechanism of failure and instability of ecological reinforced soil-retaining walls, dynamic characteristics, stability analysis methods, and durability.

However, the studies on the mechanical properties of the reinforced soil interface after dry-wet cycles are very few. In order to study the effects of the dry-wet cycle and moisture content on the mechanical properties of the reinforced soil interface, this study conducts the dry-wet cycle test and pull-out test of the reinforced soil.

2. Experiment Schemes

2.1. Equipment and Design. We used a microcomputer-controlled electrohydraulic servo universal testing machine WAW-300 and a test box of 320 mm × 300 mm × 300 mm (length × width × height), as shown in Figure 1. The horizontal pullout force was controlled by the computer with the displacement rate of 1 mm/min, and the overburden pressure was controlled by the same size concrete block, which was placed on the steel pressure plate in the test box. The front wall of the test box had a narrow slit of 210 mm × 5 mm for the grid leading out, and the hole was drilled at the bottom of the test box. 20 pores with 10 mm diameter were distributed at the bottom of the test box evenly, as shown in Figures 2–4. A 315 mm × 295 mm × 5 mm pressure-bearing steel plate was placed horizontally on the top of the test box filler so that the concrete block can apply normal stress uniformly. The universal testing machine and reinforced soil in the test box were connected by a steel wire rope, a clamp, and a guide pulley. The clamp was composed of two steel plates and bolts.

2.2. Test Materials. The fill used in the test was taken from the silty clay of Zhengzhou City, and a small pore-size (2 mm) mesh screen was used to remove impurities such as grass branches and gravel mixed in the clay. The physical and mechanical parameters are shown in Table 1.

The particle size distribution of the silty clay is shown in Table 2.

The test used glass fiber two-way geogrid, and its main technical indicators are shown in Table 3.

2.3. Test Conditions. We selected the reinforced soil samples with water content of 4%, 8%, 14%, and 20% and set the number of dry-wet cycles to 0, 7, and 30, respectively. We chose 5 types of overburden pressure with 1 kPa, 2 kPa, 3 kPa, 4 kPa, and 5 kPa, respectively, and 60 working conditions totally in the test.

2.4. Test Procedure. The specific experimental process is shown in Figure 5.

(1) Customize two steel test tanks. The clearance size of the test tank is as follows: length × width × height = 320 mm × 300 mm × 300 mm. There is a 210 mm ×

Figure 1: The reinforced soil pull-out test.

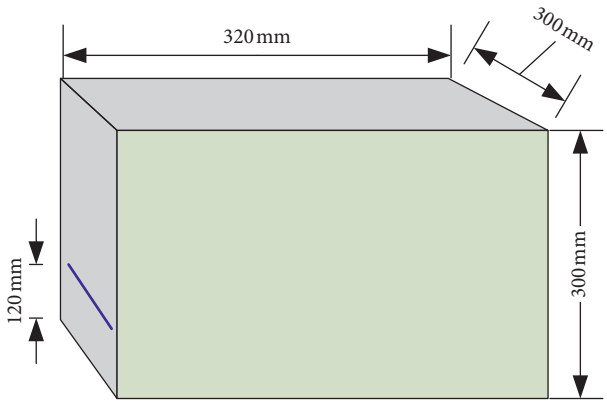

Figure 2: The schematic diagram of the test box.

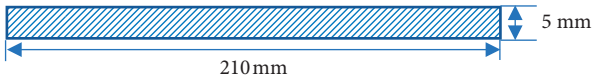

Figure 3: The schematic diagram of the narrow slit of the test box.

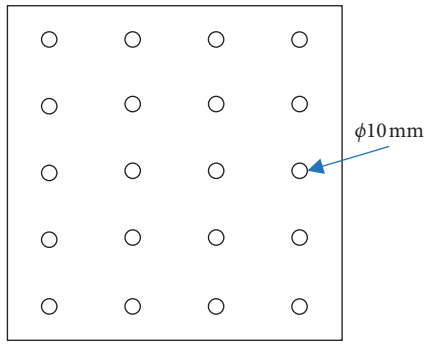

Figure 4: The schematic diagram of punching holes at the bottom of the test box.

Table 1: Filler physical and mechanical parameters.

Parameter	Symbol/unit	Value
Unit weight	γ/kN·m^{-3}	19
Elastic modulus	E/MPa	20
Poisson's ratio	μ	0.35
Cohesion	c/kPa	15
Interface friction angle	φ/°	20
Dilation angle	ϕ/°	0
Optimum moisture content	%	17.1
Maximum dry density	kN/m^3	1.76
Liquid limit	%	43.7
Plasticity index	—	13.7

Table 2: The particle size of the silty clay.

Particle size (mm)	Gradation (%)
≤0.005	10
0.005–0.01	30
0.01–0.015	40
0.015–0.02	15
0.02–0.025	5

10 mm slit in the front of the test box for the grid leading out. The box height is 300 mm. In order to hold the box, the upper part of the box (about 60 mm height) is empty. And, the silty clay in the box is only 240 mm. So, the narrow slit at a distance of 120 mm from the bottom is placed at the mid-height of the silty clay in the box. Punch holes at the bottom of the test box. The pore diameter is 10 mm. 20 holes are evenly distributed at the bottom of the test box, as shown in Figures 2–4.

(2) Use a mesh screen with a small aperture (2 mm) to remove impurities such as grass branches and gravel in the silty clay.

Table 3: Main technical indicators of the geogrid.

Reinforced material	Breaking strength (kN/m)		Elongation at break		Grid size (mm∗mm)	Mass per unit area (g/m^2)	Rib thickness (mm)
EGA100-100	Radial	Weft direction	Radial	Weft direction	25.4∗25.4	120	1.5
	103.5	102.8	3.0	3.0			

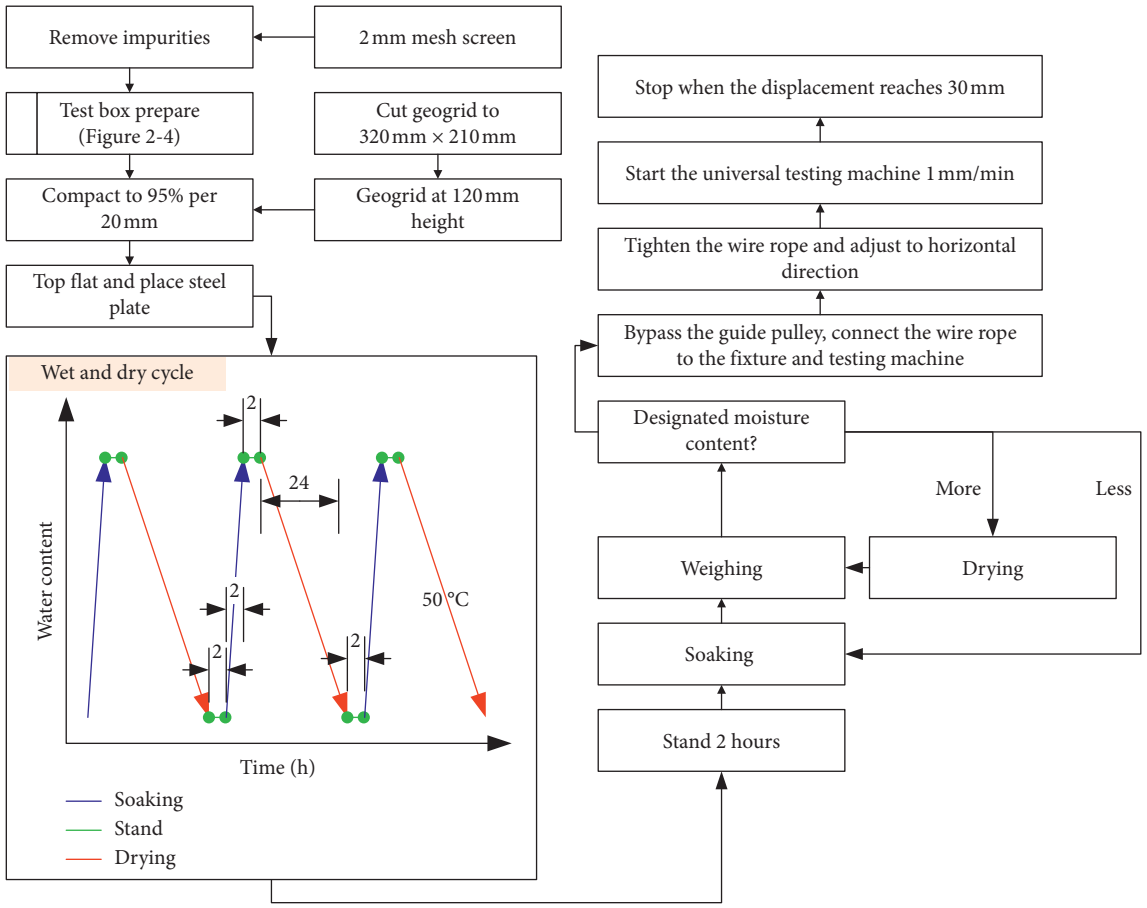

Figure 5: The experimental flowchart.

(3) Cut the glass fiber geogrid to the size of 320 mm × 210 mm.

(4) Carry out the dry-wet cycle, and the reinforced soil dry-wet cycle is divided into three working conditions: ① no dry-wet cycle; ② seven dry-wet cycles; ③ thirty dry-wet cycles. The dry-wet cycles are carried out by the soaking and drying process. First, put the geotextile at the bottom of the test box. Second, put the reinforced soil in the test box and compact it. Finally, put the test box in the water tank, and the height of the water tank should not exceed the narrow slit of the test box. After 2 hours of immersion, the test box is taken out of the water tank with standing for 2 hours. Then, the reinforced soil is put on the tray of the dryer, with the temperature of 50°C and drying time of 24 h. Reinforced soil samples after 0, 7, and 30 dry-wet cycles are used for pull-out tests.

(5) Add the silty clay that has undergone dry-wet cycles to the test box, and compact it for every 20 mm height. Ensure that the compaction is 95% each time.

(6) When the silty clay is added and compacted to the height of 120 mm, put the geogrid specimens into the test box with accurate position, and then, continue to add the silty clay and compact by layers.

(7) After compacting to the specified height, first level the top, and then, place the steel bearing plate and concrete blocks according to different overlying pressure requirements. Carry out the pull test after 2 hours of standing.

(8) Start the universal testing machine, using two steel plates and bolts to fix the geogrid, connecting one end of the wire rope to the fixture, bypassing the guide pulley, and then connecting the other end of the wire rope to the fixture of the universal testing machine.

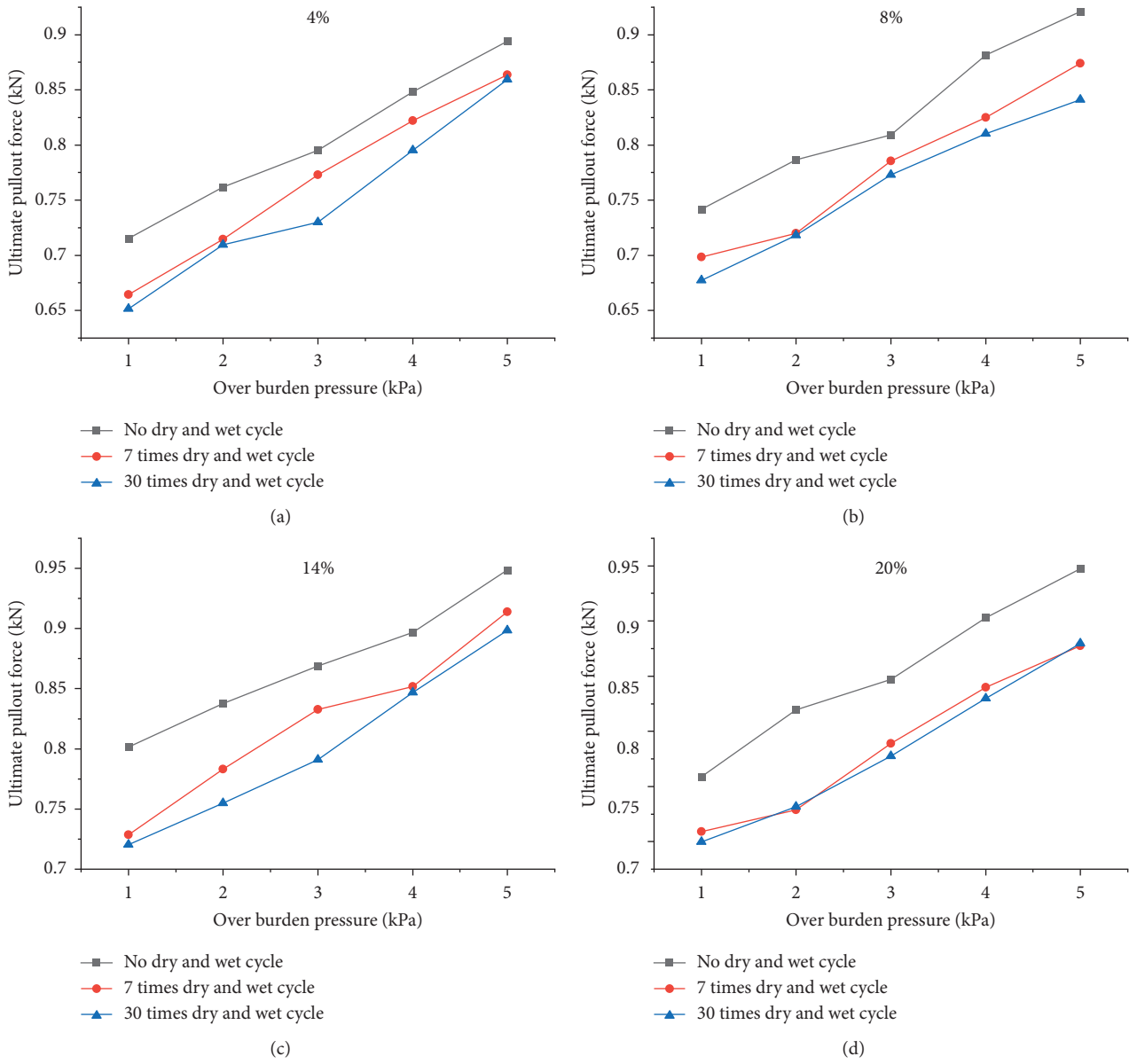

Figure 6: The ultimate pullout force-overlying pressure curve with different water content for dry-wet cycles.

(9) Install the guide pulley on the fixture of the universal testing machine, adjusting the position of the test box, tightening the wire rope, and making the narrow slot of the test box and guide pulley in the same horizontal direction.

(10) Start the universal testing machine software and set the relevant parameters so that the geogrid is drawn with the speed of 1 mm/min. When the drawing displacement reaches the value of 30 mm, the test will be stopped, and the data will be saved.

(11) Repeat the above steps for the next working condition to measure parameters of the geogrid and fill interface under different dry-wet cycles, different moisture content, and different overlying pressure conditions.

3. Test Results and Analysis

3.1. Analysis of the Change of Ultimate Pullout Force under the Action of Dry-Wet Cycles. The ultimate pullout force-overlying pressure curve with different water content for dry-wet cycles is shown in Figure 6.

It can be seen from Figure 6 that when the water content and number of dry-wet cycles are fixed, the ultimate pullout force of the reinforced soil overall linearly increases with the increase of overburden pressure because the overburden pressure makes the friction resistance of the soil and reinforcement interface increase. Different water content has little effect on the ultimate pullout force-overlying pressure curve. When the water content and overburden pressure are constant, the ultimate pullout force of the reinforced soil decreases with the increase of the number of dry-wet cycles.

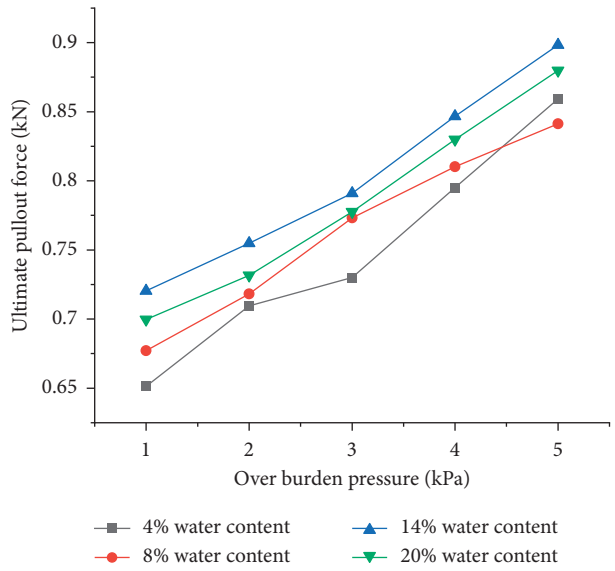

Figure 7: The ultimate pullout force-overburden pressure curve with different water content for 30 dry-wet cycles.

After 7 dry-wet cycles, the ultimate pullout force decreases obviously. And, after 30 dry-wet cycles, the ultimate pullout force decreases less. When the overburden pressure is 5 kPa and water content is 4%, the ultimate pullout force of the reinforced soil is 0.894 kN without the dry-wet cycle. After 7 dry-wet cycles, the ultimate pullout force of the reinforced soil is reduced by 3.4%. After 30 dry-wet cycles, the ultimate pullout force of the reinforced soil is reduced by 3.88%. When the overburden pressure is 5 kPa and water content is 8%, the ultimate pullout force of the reinforced soil is 0.9211 kN without dry-wet cycles, while the ultimate pullout force of the reinforced soil is reduced by 5.11% after 7 dry-wet cycles. After 30 dry-wet cycles, the ultimate pullout force of the reinforced soil is reduced by 8.66%. When the overburden pressure is 5 kPa and water content is 14%, the ultimate pullout force of the reinforced soil is 0.9486 kN without the dry-wet cycle, and after 7 dry-wet cycles, the ultimate pullout force of the reinforced soil is reduced by 3.86%. After 30 dry-wet cycles, the ultimate pullout force of the reinforced soil is reduced by 5.3%. When the overburden pressure is 5 kPa and water content is 20%, the ultimate pullout force of the reinforced soil is 0.9475 kN without the dry-wet cycle, and the ultimate pullout force of the reinforced soil is reduced by 7.39% after 7 dry-wet cycles. After 30 dry-wet cycles, the ultimate pullout force of the reinforced soil is reduced by 7.15%. It shows that after 7 dry-wet cycles, the number of cycles has little effect on the ultimate pullout force of the reinforced soil.

The ultimate pullout force-overburden pressure curve with different water content for 30 dry-wet cycles is shown in Figure 7.

When the overburden pressure is constant and water content is 14%, the ultimate pullout force of the reinforced soil is maximum. When the overburden pressure is 5 kPa, the ultimate pullout force is 0.8983 kN with water content of 14%. When the overburden pressure is constant and water content is 4%, the ultimate pullout force of the reinforced soil is the minimal except for the overburden pressure of 5 kPa. When the overburden pressure is 5 kPa and water content is 8%, the ultimate pullout force is 0.8413 kN, which is minimal. This is 6.35% lower than the ultimate pullout force with the water content of 14%. When the overburden pressure is constant, the corresponding water content of reinforced soils with ultimate pullout force values from big to small is 14%, 20%, 8%, and 4%, respectively, except for the overburden pressure of 5 kPa.

3.2. Relationship between Pull-Out Force and Pull-Out Displacement under the Action of Dry-Wet Cycles. When the overburden pressure is 5 kPa, the pullout force-displacement curve with different water content for different dry-wet cycles is shown in Figure 8.

It can be seen from Figure 8 that when the number of dry-wet cycles and water content are fixed, the pullout force increases with the increase of the drawing displacement, and the pullout force-displacement curve can be divided into two stages. In the first stage, the drawing displacement is in a very small range. The pullout force increases rapidly and linearly. In the second stage, the pullout force increases slightly and then tends to be stable after reaching the limitation. In the first stage of the pullout force-displacement curve, the geogrid is not completely pulled out, so the pullout force increases rapidly. In the second stage of the pullout force-displacement curve, the geogrid is completely pulled out, and the interaction between the geogrid and fill becomes a sliding friction. So, the pullout force is stable. When the water content is constant, the pullout force decreases with the increase of dry-wet cycles. When the water content is 4% and 8%, the first stage linear slope of the pullout force-displacement curve decreases with the increase of dry-wet cycles. When the water content is 14% and 20%, the slope does not change too much with the increase of dry-wet cycles. It shows that when the water content is 14% and 20%,

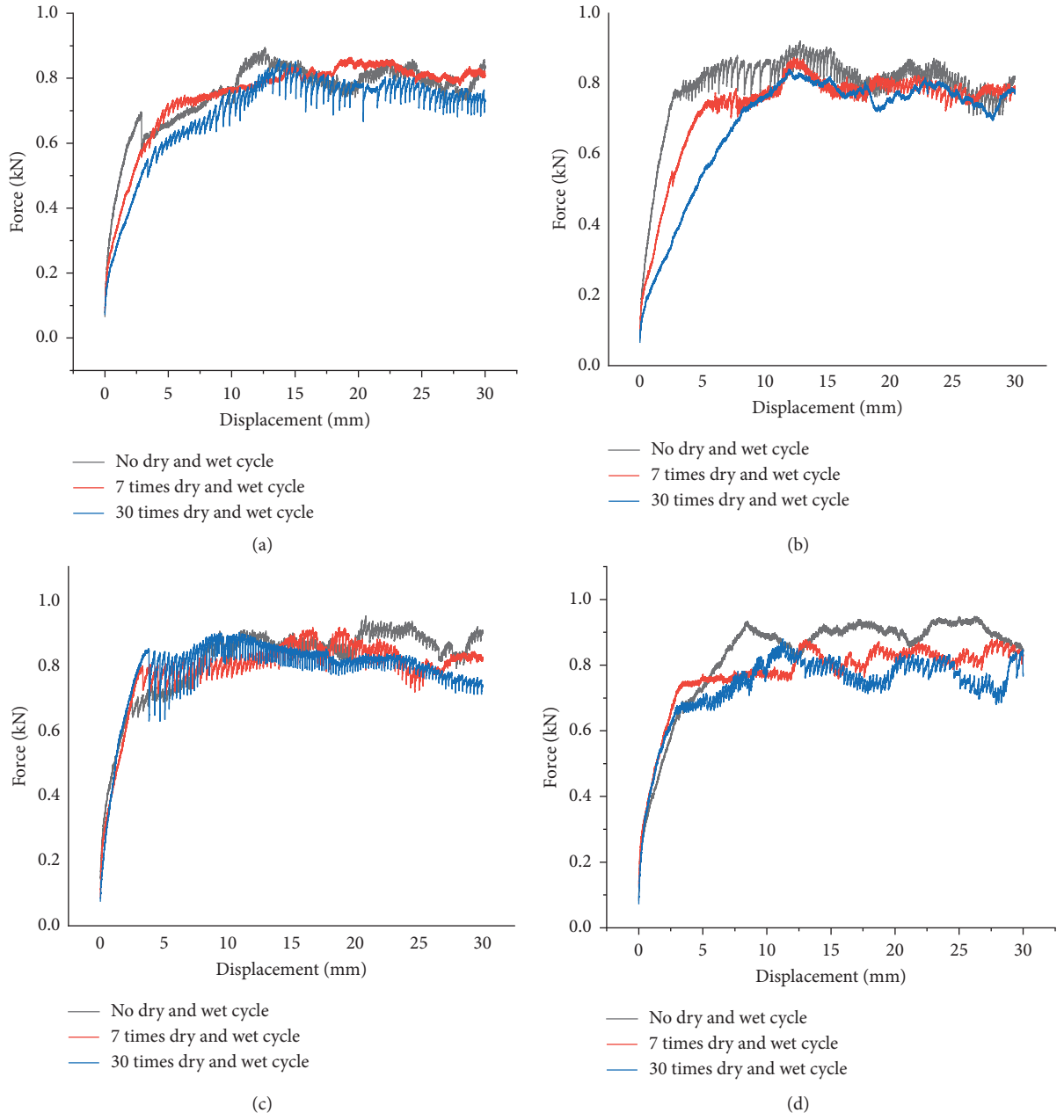

Figure 8: The pullout force-displacement curve with different water content for dry-wet cycles under the overburden pressure of 5 kPa. (a) 4%. (b) 8%. (c) 14%. (d) 20%.

the interaction between the geogrid and fill is stronger. The change of water content has little effect on the trend of the pullout force-displacement curve. The force-displacement curve of the reinforcement-soil interface fluctuates due to the aging of the experimental instrument fixture, but it does not affect the overall trend of the observation curve.

Figure 9 is the pullout force-displacement curve with different water content for 30 dry-wet cycles under overburden pressure of 5 kPa.

As can be seen from Figure 9, when the water content is 14% for 30 dry-wet cycles, the first stage linear slope of the pullout force-displacement curve is maximum. It shows that the interaction between the geogrid and fill is the strongest when the water content is 14%. The first stage linear slope of the pullout force-displacement curve from big to small correspond to the water content values of 14%, 20%, 4%, and 8%, respectively.

When the water content is 14%, the pullout force-displacement curve for 30 dry-wet cycles under different overburden pressures is shown in Figure 10.

It can be seen from Figure 10 that the first stage linear slope of the pullout force-displacement curve increases with the increase of the overburden pressure. It shows that the interaction between the geogrid and fill is related to the overburden pressure. As the overburden pressure is greater, the interaction between the geogrid and fill is stronger. The

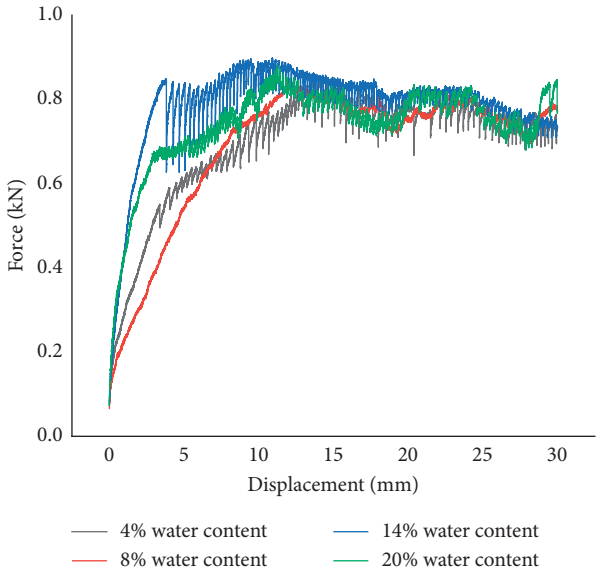

Figure 9: The pullout force-displacement curve with different water content for 30 dry-wet cycles under overburden pressure of 5 kPa.

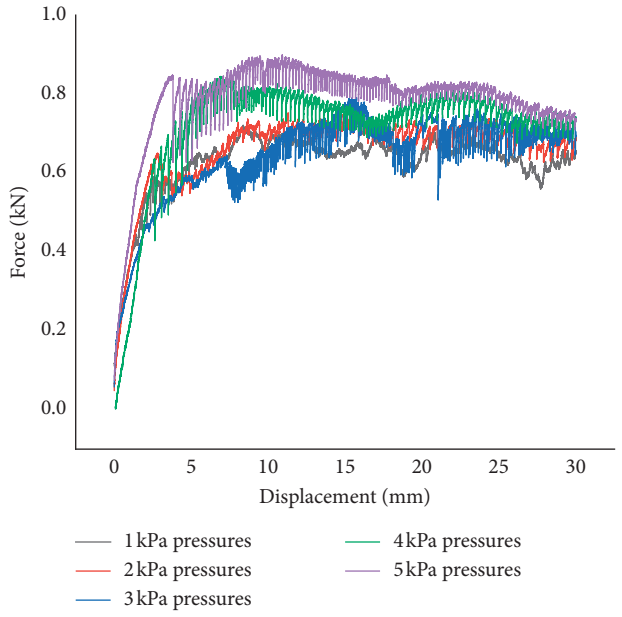

Figure 10: The pullout force-displacement curve with water content of 14% for 30 dry-wet cycles under different overburden pressure.

pullout force of the reinforced soil increases with the increase of the overburden pressure.

3.3. Analysis of Shear Stress and Normal Stress. The maximum shearing strength τ which measured the soil-reinforcement interface can be obtained from the ultimate pullout force test. Assuming that the friction between the fill and geogrid is evenly distributed, it can be solved using equation (1):

$$\tau = \frac{T}{2B(L-d)}, \tag{1}$$

where T is the ultimate pullout force in the pullout test of the reinforced soil (kPa), B and L are the width and length of the interface between the geogrid and fill, and $B = 0.2$ m, $L = 0.25$ m, and d is the pull-out length (m).

The normal stress σ of the pull-out test can be solved by formula (2):

$$\sigma = P_1 + P_2 + \gamma h, \tag{2}$$

where P_1 is overlay pressure applied on the reinforced earth steel pressure plate (kPa), P_2 is the weight of the steel pressure-bearing plate (0.2 kPa), γ is the bulk density of the fill 13.8 kN/m^3, 14.4 kN/m^3, 15.2 kN/m^3, and 16 kN/m^3, corresponding bulk density of water content 4%, 8%, 14%, and 20%, respectively, and h is the height of the earth fill on the geogrid (0.1 m).

Through formulae (1) and (2), the shear stress and normal stress can be obtained under different dry-wet cycles and different water content, and the relationship between shear stress and normal stress can be obtained by fitting $\tau = \sigma \tan \varphi + c$, as shown in Table 4.

When the water content is different, the relationship between shear stress and normal stress of the reinforced soil for different dry-wet cycles is shown in Figure 11.

It can be seen from Table 4 and Figure 11 that when the number of dry-wet cycles is fixed, the shear stress of the reinforced soil is linearly related to the normal stress with different water content. When the number of dry-wet cycles is fixed, the interface friction angle of the reinforced soil first decreases and then increases with the increase of water content. When the number of dry-wet cycles is 0 and 7, the interface friction angle of the reinforced soil is the minimal with the water content of 14%. The apparent cohesion of the reinforced soil first increases and then decreases with the increase of the water content. When the water content is 14%, the apparent cohesion of the reinforced soil is the maximum. The maximum apparent cohesion of the reinforced soil decreases with the increase of the number of dry-wet cycles, and the minimum interface friction angle increases with the increase of the number of dry-wet cycles.

When the water content is 14%, the shear stress-normal stress curve for different dry-wet cycles is shown in Figure 12.

It can be seen from Figure 12 that when the water content is 14%, the slope of the curve, that is, the interface friction angle, does not change significantly with the increase in the number of dry-wet cycles, especially the slope after 7 dry-wet cycles. The apparent cohesion of the reinforced soil decreases with the increase of the number of dry-wet cycles. The difference of the apparent cohesion between the 7th and 30th dry-wet cycle is about 0.2 kPa, which shows that after 7 dry-wet cycles, the apparent cohesion was little affected. The apparent cohesion of the reinforced soil after 0th dry-wet cycle is 7.0370 kPa, and the apparent cohesion after 7 dry-wet cycles is 6.1451 kPa, which is a decrease of 12.7%.

Table 4: Relationship between shear stress and normal stress.

Cycle times (times)	Water content (%)	Fitting formula	Interface friction angle (°)	Fit index
0	4	$\tau = 0.4435\sigma + 5.9983$	23.92	0.9947
	8	$\tau = 0.4535\sigma + 6.1768$	24.39	0.9701
	14	$\tau = 0.3536\sigma + 7.0370$	19.47	0.9843
	20	$\tau = 0.4604\sigma + 6.3421$	24.72	0.9880
7	4	$\tau = 0.5055\sigma + 5.3604$	26.82	0.9959
	8	$\tau = 0.4562\sigma + 5.6888$	24.52	0.9789
	14	$\tau = 0.4396\sigma + 6.1451$	23.73	0.9737
	20	$\tau = 0.4480\sigma + 5.7380$	24.13	0.9753
30	4	$\tau = 0.5015\sigma + 5.1941$	26.63	0.9693
	8	$\tau = 0.4202\sigma + 5.6905$	22.79	0.9873
	14	$\tau = 0.4475\sigma + 5.9104$	24.11	0.9844
	20	$\tau = 0.4584\sigma + 5.6367$	24.63	0.9903

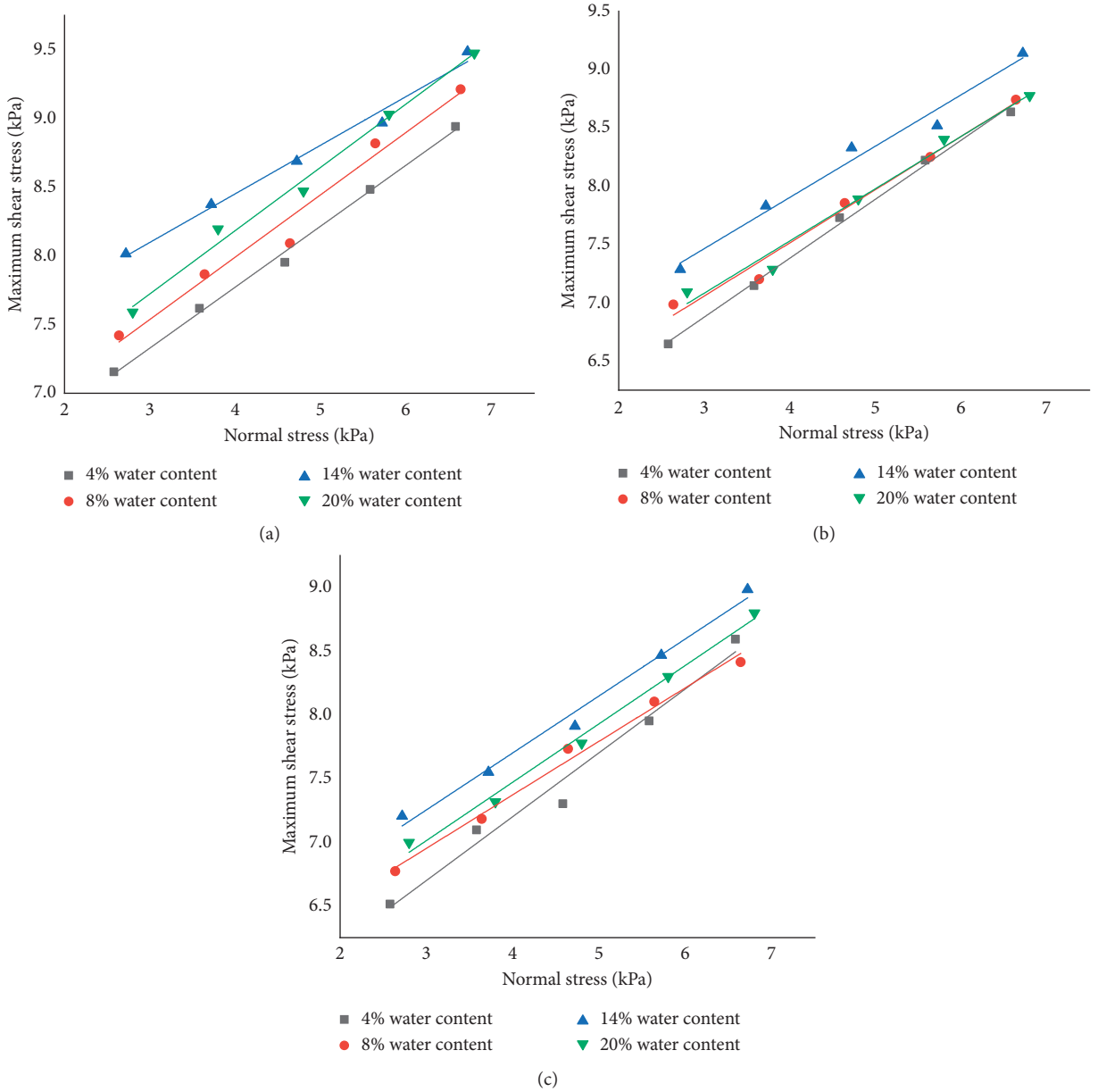

Figure 11: The maximum shear stress-normal stress curve for different dry-wet cycles with different water content. (a) 0 times. (b) 7 times. (c) 30 times.

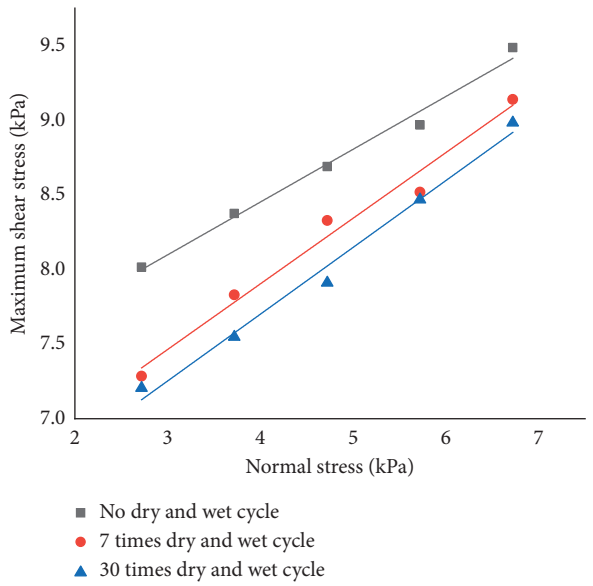

Figure 12: The maximum shear stress-normal stress curve for different dry-wet cycles with water content of 14%.

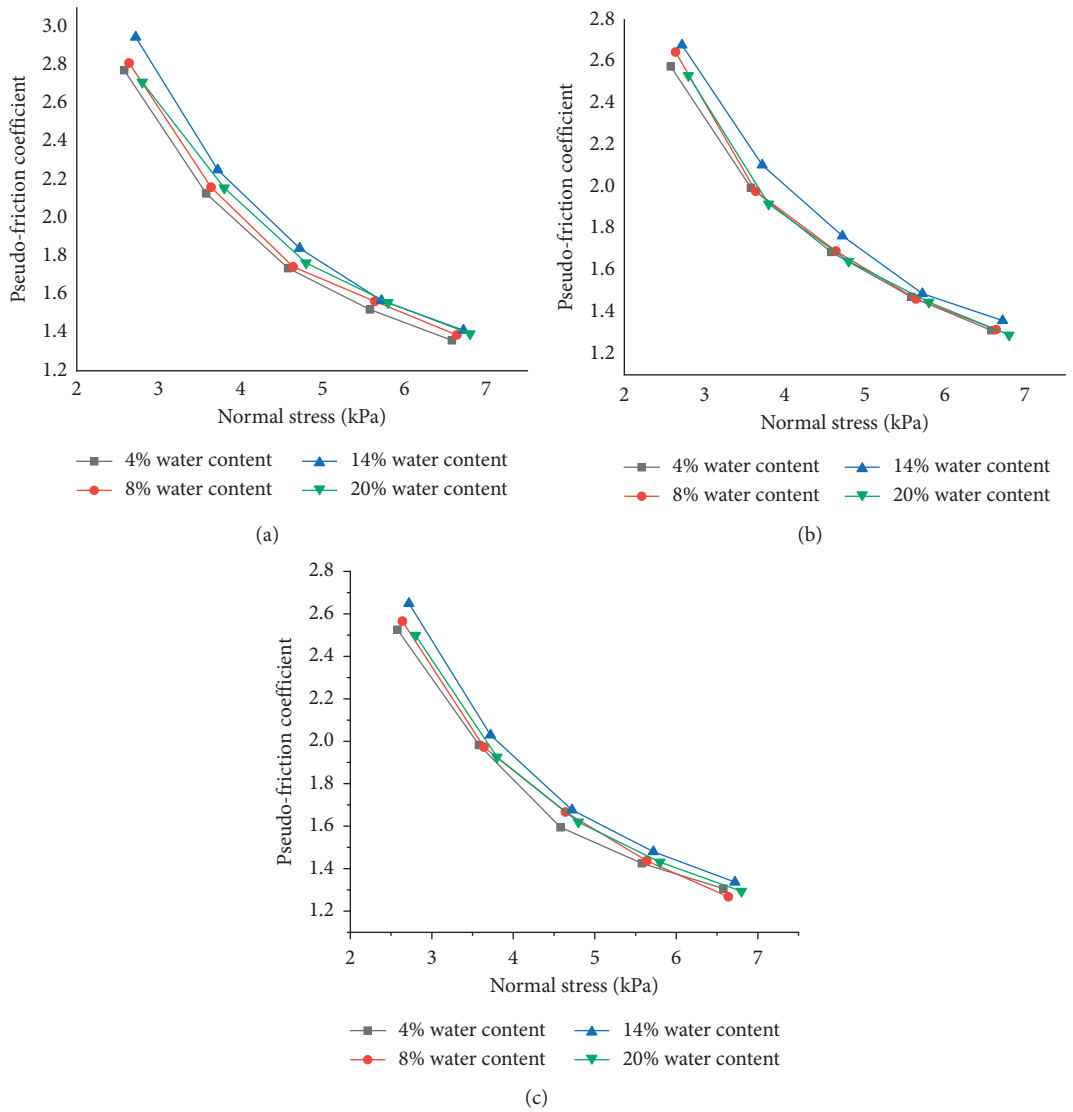

Figure 13: The apparent friction coefficient-normal stresses curve with different water content for different dry-wet cycles. (a) 0 times. (b) 7 times. (c) 30 times.

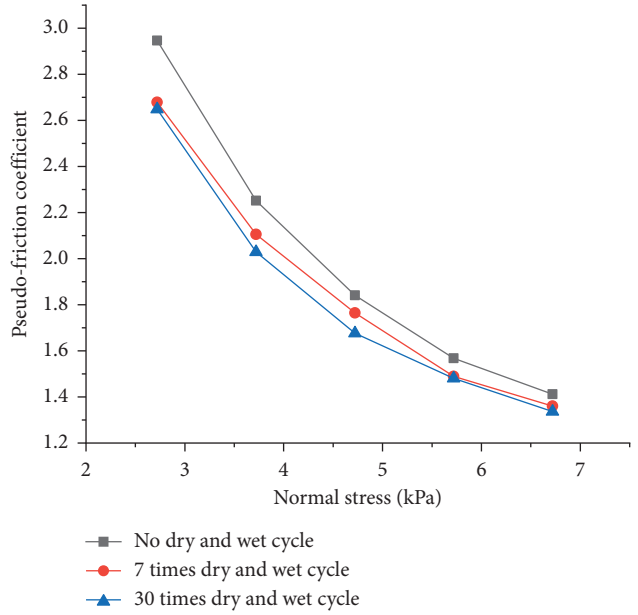

Figure 14: The apparent friction coefficient-normal stresses curve for different dry-wet cycles with water content of 14%.

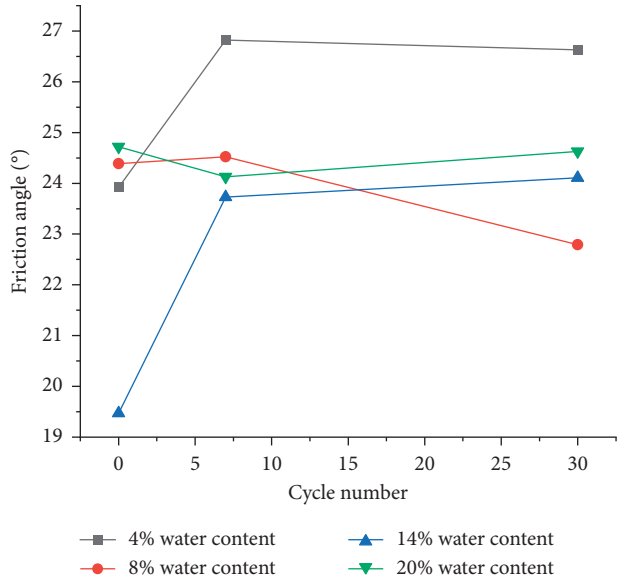

Figure 15: The friction angle-cycle number curve with different water content.

3.4. Relationship between Apparent Friction Coefficient and Normal Stress. The interface characteristics of the reinforced can be reflected by the apparent friction coefficient, which can reflect the interaction between the geogrid and fill. The formula for calculating the apparent friction coefficient is as follows:

$$f = \frac{\tau}{\sigma}, \tag{3}$$

where τ and σ are the maximum shear stress and normal stress in the pullout test of the reinforced soil, respectively (kPa).

The apparent friction coefficient-normal stresses curve with different water content for different dry-wet cycles is shown in Figure 13.

It can be seen from Figure 13 that the number of dry-wet cycles and water content do not affect the apparent friction coefficient-normal stresses curve. When the number of dry-wet cycles and water content is fixed, the apparent friction coefficient decreases with the increase of normal stress. When the number of dry-wet cycles and normal stress is constant, the apparent friction coefficient corresponding water content from big to small is 14%, 20%, 8%, and 4%, respectively. When the water content is 14% and normal

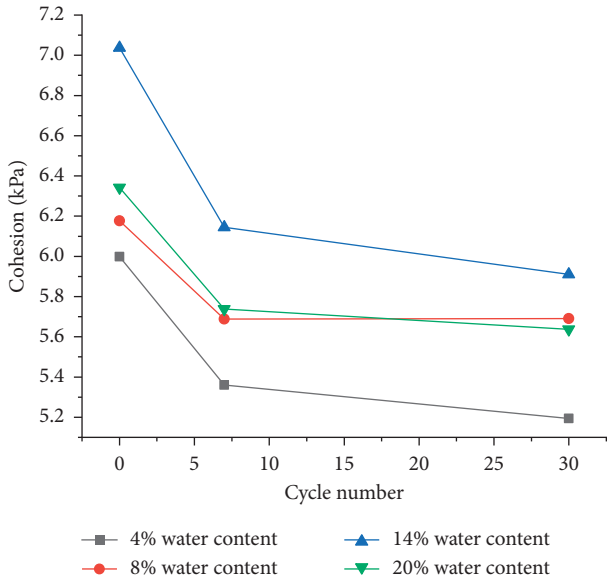

Figure 16: The cohesion-cycle number curve with different water content.

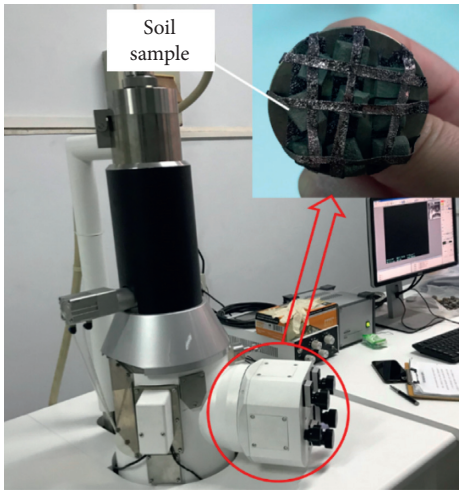

Figure 17: The scanning electron microscope and soil samples.

stress is the minimum, the apparent friction coefficient is the maximum. When the number of dry-wet cycles is 0, 7, and 30, the corresponding apparent friction coefficient is 2.95, 2.68, and 2.65, respectively.

Figure 14 is the apparent friction coefficient-normal stresses curve for different dry-wet cycles with water content of 14%.

It can be seen from Figure 14 that when the normal stress is constant and water content is 14%, the apparent friction coefficient decreases with the increase of the number of dry-wet cycles. After 7 and 30 dry-wet cycles, the difference of the apparent friction coefficient of the interface is not significant. This means that 7 dry-wet cycles have little effect on the apparent friction coefficient. When the normal stress is minimal, the apparent friction coefficient is 2.95 without dry-wet cycles. The coefficient is 2.68 after 7 dry-wet cycles, which reduced by 9.2%. After 30 dry-wet cycles, the apparent friction coefficient is 2.65, with 10.2% decrease. This shows that the interaction between the geogrid and fill will decrease after dry-wet cycles.

3.5. Analysis of Changes in the Apparent Cohesion and Friction Angle of the Soil-Reinforcement Interface. The dry-wet cycle test and pull-out test of the reinforced soil can obtain the apparent cohesion and friction angle of the soil-reinforcement interface under different working conditions. The friction angle-cycle number curve with different water content is shown in Figure 15. The cohesion-cycle number curve with different water content is shown in Figure 16.

Figure 15 shows that comparing the 0 to 7 dry-wet cycles and the 7 to 30 dry-wet cycles, the slope of the friction angle of the soil-reinforcement interface (change rate) has a significant change at 7 dry-wet cycles because dry-wet cycles cause the structure of the reinforced soil to be reconstructed,

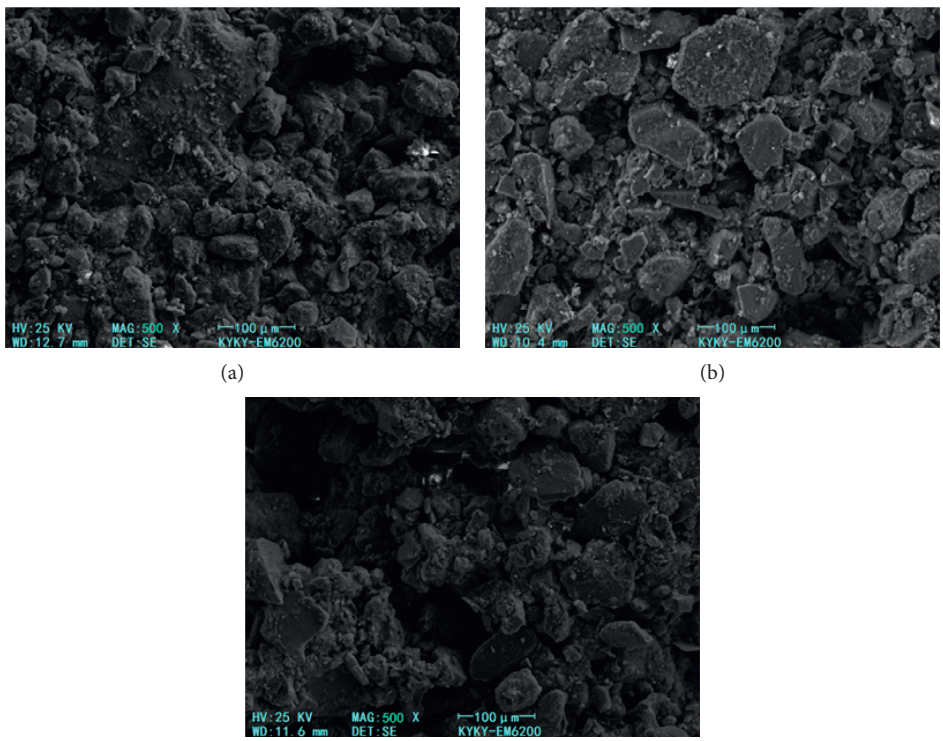

(a) (b)

(c)

Figure 18: Microstructure of the reinforced soil after different number of dry-wet cycles. (a) 0 times. (b) 7 times. (c) 30 times.

and the changes of the friction angle of the soil-reinforcement interface corresponding to different water content before the 7 dry-wet cycles reflect the instability of its reconstruction. While the change of the friction angle of the soil-reinforcement interface corresponding to the 7 to 30 dry-wet cycles is small, it means that the reconstruction of the reinforced soil has stabilized. An exception is that the moisture content is 20%, which indicates that excessive moisture content will lead to further reconstruction of the reinforced soil pores.

It can be seen from Figure 16 that with different water content, the apparent cohesion of the soil-reinforcement interface decreases with the increase of the number of dry-wet cycles. Water content has little effect on the trend of the cohesion-cycle number curve. The apparent cohesion of the soil-reinforcement interface first decreases greatly after 7 dry-wet cycles and then decreases slowly after 30 dry-wet cycles. After 30 dry-wet cycles, the apparent cohesion of the soil-reinforcement interface with water content of 4% is the minimum, 5.19 kPa, and the apparent cohesion of the soil-reinforcement interface with water content of 14% is the maximum, 5.91 kPa. The apparent cohesion of the soil-reinforcement interface from big to small corresponds to the water content of 14%, 20%, 8%, and 4%. When the water content is 8% and 20%, the apparent cohesion of the soil-reinforcement interface is similar.

3.6. Microstructure Analysis. In order to study the microstructure of the reinforced soil before and after different dry-wet cycles and analyze the relationship between the microstructure of the reinforced soil and number of dry-wet cycles, we used a scanning electron microscope to observe the reinforced soil sample. After 0, 7, and 30 dry-wet cycles, a small piece of the reinforced soil was dried first and then sprayed with gold to make it conducive. After the reinforced soil sample was prepared, it was placed in a scanning electron microscope for observation, as shown in Figure 17.

The magnification of this electron microscope test was 500 times. The reinforced soil samples after different dry-wet cycles were scanned by the electron microscope. The microstructure is shown in Figure 18.

It can be seen from Figure 18 that without dry-wet cycles, the reinforced soil has a small gap and close contact. Small gap and close contact leads to large cohesion of the reinforced soil. After 7 dry-wet cycles, the gap between the reinforced soil particles increases significantly, and the number of pores increases greatly. And, this leads to the decrease of the cohesion of the reinforced soil. The gap between the reinforced soil particles after 30 dry-wet cycles has no significant difference comparing with that after 7 dry-wet cycles. And, this shows that there are no significant differences in cohesion after 7 dry-wet cycles and 30 dry-wet cycles. This verifies the law of the apparent cohesion of the soil-reinforcement interface obtained from the dry-wet cycle test and pull-out test.

4. Conclusion

Based on the reinforced soil pullout test, the effects of different dry-wet cycles, different water content, and different overburden pressure on the mechanical properties of the reinforced soil interface are studied. The overall conclusions are as the following.

(1) The ultimate pullout force of the reinforced soil increases linearly with the increase of overburden pressure and decreases with the increase of the number of dry-wet cycles. When the overburden pressure is 5 kPa and water content is 14%, the ultimate pullout force of the reinforced soil decreases by 5.3% after 30 cycles of dry-wet cycles.

(2) The pullout force increases with the increase of the drawing displacement, and the drawing curve can be divided into two stages. In the first stage, the pullout force increases rapidly within a very small range of the drawing displacement and overall linear growth. The pullout force in the second stage increases slightly, and the pullout force tends to be stable after reaching the limit pullout force.

(3) The shear stress of the reinforced soil is linearly related to the normal stress, and the fitting index is between 0.9693~0.9959. It has a good fitting condition and is in accordance with Coulomb's law.

(4) When other conditions are constant, the interface coefficient friction of the reinforced soil decreases with the increase of the number of dry-wet cycles. When the normal stress is the minimum and water content is 14%, the interface coefficient friction of the reinforced soil after 30 dry-wet cycles is 2.65, a decrease of 10.2%. After the wet and dry cycles of the reinforced soil, the interaction between the geogrid and fill will reduce, and the friction effect of the reinforced soil after 7 dry-wet cycles is basically the same.

(5) Since dry-wet cycles can cause the reconstruction of the reinforced soil, the friction angle of the soil-reinforcement interface changes with different water content before 7 dry-wet cycles, which reflects the instability of its reconstruction. While the friction angle of the soil-reinforcement interface from 7 to 30 dry-wet cycles changes very little, it shows that the reconstruction of the reinforced soil is stable. The apparent cohesion of the soil-reinforcement interface decreases with the increase of dry-wet cycles. After 30 dry-wet cycles, the apparent cohesion of the soil-reinforcement interface with water content of 14% is the maximum, 5.91 kPa.

(6) The variation law of cohesion derived from microstructure analysis conforms to the laws and conclusions obtained by the experiment.

Data Availability

All the data included in this study are available from the corresponding author upon request.

Conflicts of Interest

The authors declare that they have no conflicts of interest regarding the publication of this paper.

Acknowledgments

This study was supported by the National Key Research and Development Program of China (2016YFE0205100).

References

[1] A. Yang, S. Jiang, F. Ankun, L. Chen, and M. Zhao, "Study on the mechanical properties of solidified light soil under dry-wet cycles and large deformation conditions," *Hydrogeology and Engineering Geology*, vol. 47, no. 3, pp. 93–100, 2020.

[2] Z. Pan, G. Yang, W. Ye, J. Tian, and B. Liang, "Study on mechanical properties and meso-damage of undisturbed loess under dry-wet cycles," *Journal of Engineering Geology*, vol. 1–7, 2020.

[3] D. Zhang and H. Rong, "Large-scale pull-out model test analysis of reinforced coarse-grained soil," *Hebei Industrial Science and Technology*, vol. 37, no. 03, pp. 196–202, 2020.

[4] H. Zhou, *Study on Mechanical Properties and Slope Stability of Red Clay under Dry-Wet Cycle*, Beijing Jiaotong University, Beijing, China, 2019.

[5] J. Liu, Y. Zhao, J. Han, Li Xin, and J. Liu, "Research on shear characteristics of fiber reinforced soil and structure interface under cyclic loading," *Water Resources and Hydropower Technology*, vol. 51, no. 1, pp. 159–165, 2020.

[6] S. Qu and Z. Yu, "Study on the physical and mechanical properties of the improved soil during the dry-wet cycle," *Shanxi Architecture*, vol. 43, no. 25, pp. 98–100, 2017.

[7] W. Liu, Q. Yang, X. Sun, and H. Yuan, "Effect of drying stress history on saturated mechanical properties of silty clay under dry-wet cycle conditions," *Journal of Hydraulic Engineering*, vol. 48, no. 2, pp. 203–209, 2017.

[8] Q. Shao, *Experimental Study on Mechanical Properties of Reinforced Soil Interface and Numerical Simulation of Particle Flow*, Qingdao Technological University, Qingdao, China, 2018.

[9] A. Pant, G. V. Ramana, M. Datta, and S. K. Gupta, "Coal combustion residue as structural fill material for reinforced soil structures," *Journal of Cleaner Production*, vol. 232, 2019.

[10] G. Cardile, M. Pisano, and N. Moraci, "The influence of a cyclic loading history on soil-geogrid interaction under pullout condition," *Geotextiles and Geomembranes*, vol. 47, no. 4, 2019.

[11] A. M. Morsy, J. G. Zornberg, J. Han, and D. Leshchinsky, "A new generation of soil-geosynthetic interaction experimentation," *Geotextiles and Geomembranes*, vol. 47, no. 4, 2019.

[12] M. Pinho-Lopes and M. de Lurdes Lopes, "Influence of mechanical damage induced in laboratory on the soil-geosynthetic interaction in inclined-plane shear," *Construction and Building Materials*, vol. 185, 2018.

[13] W. Liu, X. Cai, H. Xu, and X. Huang, "Research progress of geogrid pullout test," *Journal of the Institute of Disaster Prevention Science and Technology*, vol. 21, no. 2, pp. 15–20, 2019.

[14] C. Xiao, Y. Luo, Z. Wang, and H. Hu, "Pull-out test study on the characteristics of geogrid-sand soil interface," *Journal of Shenzhen University (Science and Technology Edition)*, vol. 36, no. 3, pp. 252–259, 2019.

[15] T. Zhang, "Analysis of the influence of large-scale direct shear instrument on the shear characteristics of the interface between reinforcement and soil," *Journal of Chuzhou Vocational and Technical College*, vol. 16, no. 4, pp. 66-67, 2017.

[16] J. Zhang and Y. Lin, "Meso-mechanism analysis of the interface characteristics of the grid-like toothed reinforced sand cushion," *Journal of Shanghai University (Natural Science Edition)*, vol. 24, no. 1, pp. 118–125, 2018.

[17] P. Punetha, P. Mohanty, and M. Samanta, "Microstructural investigation on mechanical behavior of soil-geosynthetic interface in direct shear test," *Geotextiles and Geomembranes*, 2017.

[18] S. Mousavi, "Shear strength behavior in the interface of contaminated soil with bio-diesel oil and geosynthetics," *Transportation Geotechnics*, vol. 10, 2016.

[19] X. Tang, Y. Zheng, and Y. Wang, "Research on the application of dual strength reduction method in the stability analysis of reinforced soil slopes," *Highway and Transportation Technology*, vol. 34, no. 3, pp. 14–17, 2018.

[20] F. Ferreira, C. Vieira, and M. de Lurdes Lopes, "Cyclic and post-cyclic shear behavior of a granite residual soil–geogrid interface," *Procedia Engineering*, vol. 143, pp. 379–386, 2016.

[21] Y. Wan, Q. Xue, L. Liu, and L. Y. Zhao, "The role of roots in the stability of landfill clay covers under the effect of dry–wet cycles," *Environmental Earth Sciences*, vol. 75, no. 1, pp. 1–9, 2016.

[22] F. B. Ferreira, C. S. Vieira, and M. L. Lopes, "Pullout behavior of different geosynthetics—influence of soil density and moisture content," *Frontiers in Built Environment*, vol. 6, no. 12, 2020.

[23] Z. Jiang, C. Wang, W. Xiao, and B. Ruan, "Experiment and numerical analysis of unconfined compressive strength of fiber reinforced soil," *Journal of Railway Science and Engineering*, vol. 17, no. 06, pp. 1404–1410, 2020.

[24] Z. Liu, *Experimental Study and Numerical Analysis of Dynamic and Static Mechanical Characteristics of Ecological Reinforced Earth Retaining Walls*, ZhongNan University, ZhongNan, China, 2012.